Motion of Spin-Labeled Side Chains in T4 Lysozyme. Correlation with Protein Structure and Dynamics†

Hassane S. Mchaourab,‡ Michael A. Lietzow,‡ Kalman Hideg,§ and Wayne L. Hubbell*,‡

Jules Stein Eye Institute and Department of Chemistry and Biochemistry, University of California, Los Angeles, California 90095-7008, and Central Research Laboratory, Chemistry, University of Pecs, P.O. Box 99, H-7643 Pecs, Hungary

Received February 27, 1996; Revised Manuscript Received April 16, 1996⊗

ABSTRACT: Thirty single cysteine substitution mutants of T4 lysozyme have been prepared and spin-labeled with a sulfhydryl-specific nitroxide reagent in order to systematically investigate the relationship between nitroxide side-chain mobility and protein structure. The perturbation caused by replacement of a native residue with a nitroxide amino acid was assessed from the resulting changes in biological activity, circular dichroism, and free energy of folding. The nitroxide produced context-dependent changes in stability and activity similar to those observed for substitution with natural amino acids at the same site but had little effect on the circular dichroism spectra. At solvent-exposed sites, the structural perturbation appears to be small at the level of the backbone fold. Nitroxide side-chain mobility faithfully reflects the protein tertiary fold at all sites investigated. The primary determinants of nitroxide side-chain mobility are tertiary interactions and backbone dynamics. Tertiary interactions constrain the side-chain mobility to an extent closely correlated with the degree of interaction. At interhelical loop sites, the side chains have a high mobility, consistent with high crystallographic thermal factors. On the exposed surfaces of α-helices, the side-chain mobility is not restricted by interactions with nearest neighbor side chains but appears to be determined by backbone dynamics. An unexpected result is a striking difference between the mobility of residues near the C- and N-termini of helices. These results provide the foundation for another dimension of information in site-directed spin-labeling experiments that can be interpreted in terms of the protein tertiary fold, its equilibrium dynamics and time-dependent conformational changes.

The determination of the three-dimensional structure of proteins provides a direct and powerful means to understand key aspects of their function, the physical basis of their stability, and their sequence-fold specificity. The central importance of these questions in modern structural biology has driven the development of structural techniques such as X-ray crystallography and multidimensional NMR that are capable of obtaining the atomic resolution structure of proteins in crystals and studying the structure, dynamics, and conformational properties of small proteins in solution, respectively. However, a variety of structural problems pose significant challenges to both methods. Among these are the structure and functional dynamics of membrane proteins, the structure of protein intermediate states, the solution structure of large water-soluble proteins, and chaperon−protein interactions.

A promising approach to explore these problems is the technique of SDSL[1] [for a recent review, see Hubbell and Altenbach (1994)]. SDSL involves the introduction of a spin-labeled side chain into protein sequences, usually through cysteine substitution mutagenesis followed by reaction with a sulfhydryl-specific nitroxide reagent. At the fundamental level of EPR analysis, the nitroxide in the protein is characterized by two features: its accessibility to collision with paramagnetic species in solution, essentially its solvent accessibility, and the motion of the spin-labeled side chain. In previous work, it was established that the backbone secondary structure and some aspects of its tertiary structure could be determined from the periodic variation in the accessibility of nitroxide side chains in a sequential set of spin-labeled proteins (Altenbach et al., 1990). In a limited study, it was also observed that the motional dynamics of the side chain, reflected in the EPR spectral line shape, correlates with the general feature of the protein fold (Altenbach et al., 1990). Of particular importance was the observation that side-chain dynamics provide a highly localized view of conformational changes mediating protein function on the millisecond time scale (Farahbakhsh et al., 1993; Steinhoff et al., 1994).

To interpret the line shape and its time-dependent changes in terms of local structure requires an understanding of the structural determinants of side-chain mobility in a protein. The relation between local structure, side-chain dynamics, and the spectral line shape is inherently complex since the label is attached through a number of bonds about which rotation can occur. Changes in the rate of rotation of any of these bonds will result in changes in the spectral line shape. Therefore, the analysis critically depends on the structure of the nitroxide itself and on the motional model

† Research reported here was supported by NIH Grant EY05216 (W.L.H.), NIH Training Grant EY07026 (M.A.L.), Research to Prevent Blindness (W.L.H.), Jules Stein Professorship Endowment (W.L.H.), and Hungarian National Research Foundation Grant OTKA/T017842 (K.H.).

* To whom correspondence should be addressed.

‡ University of California.

§ University of Pecs.

⊗ Abstract published in *Advance ACS Abstracts,* June 1, 1996.

[1] Abbreviations: EPR, electron paramagnetic resonance; PCR, polymerase chain reaction; NiEDDA, nickel(II) ethylenediaminediacetic acid; SDSL, site-directed spin-labeling; T4L, T4 lysozyme.

S0006-2960(96)00482-5 CCC: $12.00

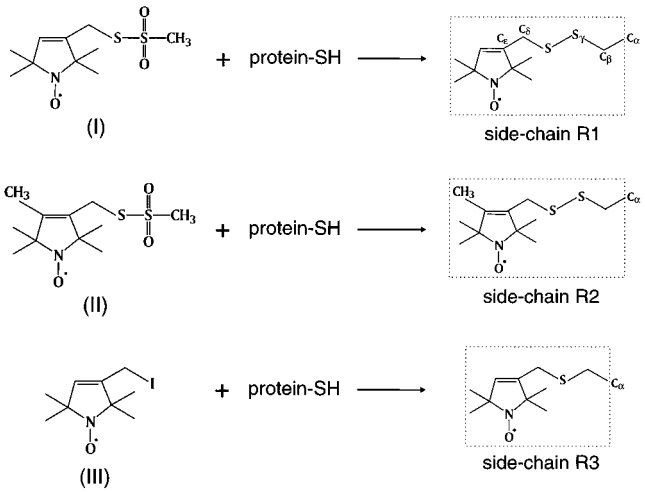

FIGURE 1: Spin-labels **I**, **II**, and **III** and the corresponding side chains R1, R2, and R3.

assumed for the internal rotation of the side chain. Most published applications of SDSL have relied on the use of the spin-label (1-oxy-2,2,5,5-tetramethylpyrrolinyl-3-methyl)-methanethiosulfonate (**I**) (Berliner et al., 1982), which reacts with cysteine residues to generate the spin-label side chain designated R1 (Figure 1). The nearly exclusive use of **I** is due to its high sulfhydryl selectivity and reactivity, the relatively small molar volume of the R1 side chain, and exquisite sensitivity of the EPR spectra to structural changes. In this paper, we initiate a detailed investigation of the structural origin of the R1 spectral line shape in T4L, a protein of accurately known structure. To aid in understanding the spectral line shapes, side chains R2 and R3, generated by reaction of cysteine with reagents **II** and **III** (Figure 1), were also investigated at a limited number of sites. The effects of local segmental flexibility, interaction with the neighboring side chain on the surface of a helix, and tertiary interactions on the motional rate and/or amplitude of the nitroxide are explored. Due to the complexity of the internal dynamics of the side chain, the goal is to understand on a coarse level the role and importance of each factor in determining the observed line shape.

The goals of SDSL are to determine protein structure at the level of the backbone fold, study equilibrium dynamics of the backbone, and resolve conformational changes in the protein fold (Hubbell & Altenbach, 1994). Therefore, it is essential for meaningful interpretation of SDSL data that the reporter group not result in significant perturbation of the secondary and tertiary organization of the protein, i.e., the backbone fold (Chothia, 1989). The question of perturbation by a nitroxide can be addressed in the general context of the tolerance of protein structure to amino acid substitutions. Matthews and co-workers have carried out a detailed and systematic mutational analysis of the factors that determine protein stability in T4L (Matthews, 1995). They determined the influence of replacing specific residues on the overall structure as well as on the free energy of folding. It was found that for surface sites amino acid substitution had little effect on stability and structure, while for buried sites the effects were dependent on the nature of the residue introduced as well as on the local context (Dao-pin et al., 1991; Eriksson et al., 1993). Mutations that affect the detailed packing of the hydrophobic core result in the largest destabilization and structural alterations. In most cases, the observed alterations involved side-chain rearrangement as well as main-chain shifts to repack the core. The overall conclusion of these studies is that destabilized mutant proteins that can fold have altered their structure in subtle ways and tend to have a backbone fold very similar to that of the wild type (Hurley et al., 1992; Baldwin et al., 1993; Matthews, 1993). Similar conclusions were reached by Sauer and co-workers, who studied in detail the tolerance of the λ repressor hydrophobic core to substitution that increases its volume (Lim et al., 1992). They found that, for introduced hydrophobic residues, modest changes in volume can be accommodated by side-chain and main-chain shifts which help relieve steric overlap by allowing the core to expand. Mutants with expanded cores retain many of the structural properties of the wild-type protein.

The mutation sites in T4L selected in this paper were chosen to explore the various structural determinants of the spectral line shape and provide a variety of contexts to determine the structural, functional, and energetic consequences of the substitution with a nitroxide. T4L is an ideal model system for this analysis because of the vast amount of thermodynamic and structural data available [for a recent review, see Matthews (1995)]. The wild-type structure of this enzyme has been refined to 1.7 Å resolution with the thermal factors included (Alber et al., 1987). T4L consists of two domains connected by a long helix. While there is some uncertainty concerning the orientation of the C-terminal domain relative to the N-terminal domain, the structure of each seems to be known with certainty (Weaver & Matthews, 1987).

In this paper, the basic properties of the spin-labeled mutants are analyzed using circular dichroism spectroscopy, in vitro biological activity, and thermal stability. The position-specific changes in the free energy of folding resulting from the substitution with R1 are compared to those resulting from substitution with a natural amino acid. The general conclusions are (1) substitution for the nitroxide side-chain R1 produces context-dependent changes in the thermal stability and enzymatic activity of T4L consistent with changes observed for substitution with natural amino acids at the same sites, (2) substitution of R1 at any site produces little change in secondary structure as judged from circular dichroism spectroscopy, (3) on solvent-exposed surfaces of an α-helix, the mobility of R1 is weakly dependent on interactions between side chains in the same helix but apparently reflects nanosecond motions of the backbone, (4) R1 residues near C-termini of helices reveal a larger amplitude of backbone motion compared to sites near N-termini, (5) exposed R1 residues in loop structures have the largest amplitude of motion, and (6) tertiary interaction sites are revealed by dramatic reductions in amplitude and/or rate of R1 motion.

MATERIALS AND METHODS

Materials. Spin-label **I** and spin-label **III** were synthesized as previously described (Berliner et al., 1982; Hankovszky et al., 1980). The synthesis of spin-label **II** will be published elsewhere. Resource S, Resource RPC, and Superdex 75 columns were obtained from Pharmacia Biotech. The cysteine-free pseudo-wild-type lysozyme gene containing the substitutions C54T and C97A (Matsumara & Matthews, 1989) was kindly provided by F. W. Dahlquist (University of Oregon). This will be referred to as the "wild type" or T4L.

Construction of T4L Mutants. Site-directed mutagenesis was performed using PCR methods. For mutants suitably located near restriction sites, synthetic oligonucleotides containing the point mutation were used to generate DNA restriction fragments. Otherwise, the overlap extension method was used as described by Ho et al. (1989). Two new restriction sites, *Xma*III and *Xba*I, were introduced into the plasmid. PCR products were ligated into the appropriate restriction sites. For all mutant constructs, the entire portion of the gene amplified was sequenced to avoid errors resulting from misincorporation by Taq polymerase. Single-site mutants are named by specifying the original residue, the number of the residue, and the new residue, in that order. Mutants with more than one substitution are identified by specifying each single mutation separated by a slash.

Expression and Purification of T4L Mutants. Mutants of T4L were expressed as previously described (Sauer et al., 1992). Briefly, mutant plasmids were used to transform competent *Escherichia coli* K38. Protein production was induced by adding isopropyl β-thiogalactoside (1 mM) to log phase cultures, and the induction was allowed to proceed for 90 min. The cells were then harvested by centrifugation, and the supernatant was discarded. Upon resuspension of the cell pellet in a buffer solution containing 25 mM Tris, 25 mM Mops, and 0.2 mM EDTA, pH 7.6, all T4L cysteine mutants appeared to initiate cell lysis. The bacterial cell wall was further disrupted under high pressure in a French press. The supernatant was then loaded on a Resource S cation-exchange column equilibrated with the same buffer and eluted with a NaCl gradient. Protein concentration was determined by UV absorption at 280 nm using an extinction coefficient of 1.228 $cm^2\ mg^{-1}$. Protein purity was analyzed by SDS−PAGE followed by silver staining, gel filtration on a Superdex 75 column, and reverse-phase chromatography on a Resource RPC column. Some mutants required further purification by gel filtration. All mutants were at least 95% pure as judged by the above analysis.

Spin-Labeling of T4L Mutants. Typically, mutant lysozymes were incubated with a 10-fold molar excess of **I**, although stoichiometric quantities are sufficient for many sites. The reaction was allowed to proceed at room temperature for at least 4 h for solvent-accessible sites and overnight for buried sites. For the latter, spin-labeling was also carried out in the unfolded state in the presence of an appropriate concentration of guanidine hydrochloride followed by refolding. Both labeling procedures yielded identical EPR spectra. For labeling of exposed sites with the spin-label **II**, a 10-fold excess was used, and the reaction was allowed to proceed overnight.

Labeling of T4L mutants with the spin-label **III** was carried out in the presence of a 10-fold excess of spin-label for 12 h. The cysteine-less WT lysozyme was also incubated with the spin-label **III** under the above conditions. It was determined that background labeling of groups other than cysteine contributed less than 10% of the total EPR signal of the labeled cysteine mutants.

Circular Dichroism. Samples for CD analysis on a Jasco J-500C spectrometer were prepared in 20 mM potassium phosphate and 25 mM KCl, pH 2.95 ± 0.05. For wavelength scans, protein concentrations were adjusted to 0.85 mg/mL. Measurements were taken at room temperature in the range of 190−260 nm. Final spectra are the averages of five scans.

For thermal denaturation, protein concentrations were adjusted to 0.1 mg/mL, and ellipticity was monitored at 223 nm. Temperature was ramped at approximately 2° per minute with a range of 10−80 °C, and data were collected at 10 s intervals. The standard deviation of the melting temperature calculated from the melting of nine different WT protein samples on different days was ±0.5 °C. All changes in melting temperature were measured with respect to a WT sample melted on the same day. The small deviations of the WT melting temperature from reported values (Blaber et al., 1994) arise from a variety of systematic errors such as the calibration of the thermocouple, temperature gradients in the sample cuvettes, and pH determination.

Activity Assays. Peptidoglycan was isolated as described in Becktel and Baase (1985) omitting the trypsin treatment. Activity assays were carried out according to Tsugita et al. (1968). Briefly, the final peptidoglycan pellet was suspended in 50 mM Tris-HCl, pH 7.4, to obtain a substrate solution with an optical density of 1.35 at 360 nm. Activity was measured as the time required for digestion of the substrate from an optical density of 1.0 to 0.9 monitored at 360 nm. Assays were run at room temperature in triplicate, and the average activities are reported.

EPR Measurements. EPR spectroscopy was performed on a Varian E-109 spectrometer fitted with a two-loop one-gap resonator (Hubbell et al., 1987). Samples of 5 μL were loaded in 0.84 mm o.d. capillaries which were sealed on both ends. All spectra were acquired using a 2 mW incident microwave power and ca. 1 G field modulation amplitude at 100 kHz.

For lysozyme, the rotational correlation time, τ_R, can be estimated from the Stokes−Einstein relation to be about 6 ns. To examine the motion of the nitroxide relative to the protein, it is desirable to reduce the contribution of protein rotation to the EPR spectral line shape. This was achieved by recording spectra in 30% w/w sucrose, which increased the protein rotational correlation time by about a factor of 3. The addition of sucrose does not affect the rotational mobility of the side chain relative to the protein at room temperature in the range of 0−40% w/w, nor does it change the value of the isotropic hyperfine constant up to 65% w/w (Timofeev & Tseltin, 1983).

The collision frequency of the nitroxide with the paramagnetic reagent NiEDDA was measured by the power saturation method (Altenbach et al., 1989).

RESULTS

Thirty single cysteine substitution mutants were prepared, and each reacted essentially quantitatively with the spin-label **I** to generate proteins containing the R1 side chain. The points of introduction were selected to represent distinct topographical sites in the T4L fold based on the crystal structure of the protein (Weaver & Matthews, 1987). These may be classified as (1) sites on the solvent-exposed surface of α-helices, not in the N- or C-cap regions, where there is little or no tertiary interaction of the side chain with other parts of the structure, (2) solvent-exposed sites near N- and C-termini of α-helices, (3) sites in solvent-exposed loop structures, (4) sites completely buried in the solvent-inaccessible hydrophobic core, and (5) sites on α-helices having various degrees of tertiary interaction with nearby structures. The latter are distinguished from buried sites by having some degree of solvent exposure.

Table 1: Enzymatic Activity of Spin-Labeled Mutants

class	mutant	activity[a]	class	mutant	activity[a]
helix	S44R1	113	loop	E22R1	55
surface	K65R1	117		K35R1	95
	N69R1	119		G51R1	65
	D72R1	100	tertiary	A74R1	3
	R76R1	115	interaction	V75R1	40
	V131R1	125		V87R1	13
	N132R1	60		N81R1	84
helix	D5R1	60		A130R1	65
N-terminal	N40R1	66		A134R1	119
	D61R1	50		I150R1	60
	A82R1	90	buried	L99R1	1.2
	T109R1	61		A129R1	11
helix	K48R1	95		L133R‘	5.5
C-terminal	R80R1	69		F153R1	7.3
	K135R1	30	side-chain	(A)65[b]	50
	D89R1	40	variants	(A)72[b]	30

[a] Percent of wild type. [b] (A)65 and A(72) are K65R1/N68A and D72R1/N68A/Q69A/R76A, respectively.

Characterization of the Spin-Labeled Mutants. The enzymatic activity of each mutant, grouped according to the classification given above, is listed in Table 1. For those with R1 at solvent-accessible sites on the surface of helices and in loops, only those close to the active site cleft or involved in substrate binding (N132, E22, A74, K135) show any significant reduction in activity. Mutants with R1 residues at exposed sites near the N- and C-termini of helices show a reduction in activity, but all have activities ≥30% of that of the wild type. Substitution for R1 at sites with tertiary interaction produces a wider range of activity changes, but all except A74R1 and V87R1 show relatively high activity. On the other hand, substitution for R1 at buried sites leads to nearly complete loss of activity. Although the side-chain R1 is of greater molar volume than any natural side chain, the effects of substitution by R1 are surprisingly similar to those for substitution of natural amino acids at the various sites, including buried sites (Matthews, 1995; Lu et al., 1992).

Although the substitution for R1 leads to substantial reduction in activity at several sites, the far-UV/CD spectra of the majority of spin-labeled mutants are essentially identical within experimental error to the wild type in the 208 and 223 nm region, as illustrated by the representative spectra in Figure 2. Only for the mutants with R1 substitutions at buried sites is there a significant decrease in the ellipticity at 198 nm. Such a decrease is common for mutations that affect the volume of the protein hydrophobic core. Significantly larger decreases have been previously reported for mutations at buried sites in thioredoxin and have been attributed to small changes in secondary structure packing (Wynn & Richards, 1993).

The degree of destabilization caused by the presence of the spin-labeled side chain was assessed by monitoring thermal unfolding with circular dichroism at 223 nm. All spin-labeled mutants studied displayed cooperative transitions, as illustrated by the representative curves in Figure 3. The melting curves were analyzed according to a two-state Van't Hoff analysis (Becktel & Schellman, 1987), and the derived thermodynamic parameters for the unfolding are shown in Table 2. For those sites that can be compared, it is notable that the values of ΔH and $\Delta\Delta G$ fall within the range of values found for substitutions at these sites by native amino acids (Matthews, 1995; Lu et al., 1992).

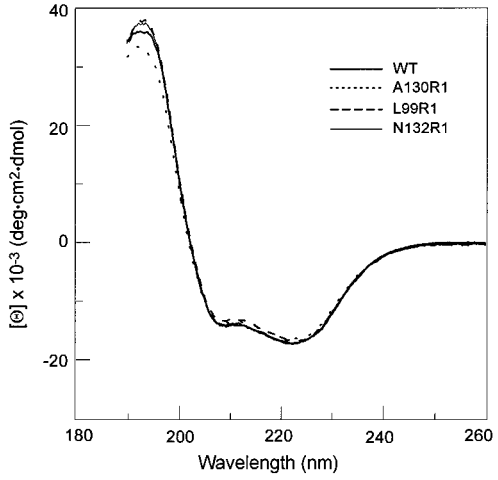

FIGURE 2: Circular dichroism spectra of T4L and representative mutants of three major structural classes: N132R1, helix surface; A130R1, tertiary interaction; L99R1, buried.

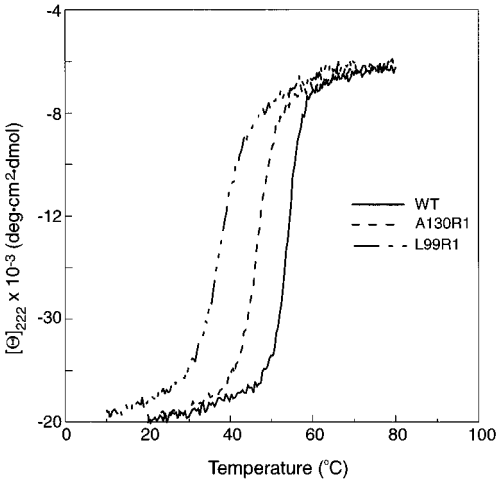

FIGURE 3: Thermal denaturation of T4L and representative mutants as measured by circular dichroism spectroscopy at 223 nm.

Dependence of Side-Chain Mobility on Protein Structure. The motion of a nitroxide side chain is reflected in the EPR spectral line shape and is related to three correlation times: (1) τ_R, the rotational correlation time for the entire protein; (2) τ_B, the effective correlation time due to rotational isomerizations about the bonds that link the nitroxide to the backbone; and (3) τ_S, the effective correlation time for segmental motion of the backbone relative to the average protein structure. These motions are assumed to be approximately independent for small-amplitude segmental fluctuations of the backbone.

The correlation time for protein rotary motion is a constant for all side chains in the folded protein. The contribution of this motion to the overall spectrum has been reduced by recording spectra in 30% sucrose solutions where the rotational correlation time is approximately 20 ns and $\tau_R > [\tau_B, \tau_S]$ for all exposed sites (see below). The effective correlation time for bond isomerizations, τ_B, is expected to depend on the primary, secondary, and tertiary structure of the protein as well as the structure of the spin-label, while τ_S is determined by the flexibility of the backbone. In the following sections, we examine the relationship between side-chain mobility, protein structure, and, for some cases, structure of the nitroxide side chain.

Rotational motions in the nitroxide side chain occur about the bonds that link it to the backbone. These bonds are in

Table 2: Thermodynamic Properties of Spin-Labeled Mutants

class	mutant	Δt_m (°C)	ΔH (kcal/mol)	$\Delta\Delta G$ (kcal/mol)
helix	S44R1	0.7	111	0.23
surface	K65R1	−1.0	115	−0.3
	D72R1	0.4	95	0.15
	V131R1	0.5	100	0.16
	N132R1	1.5	117	1.0
helix	N40R1	−1.2	100	−0.4
N-terminal	D61R1	−1.0	90	−0.32
helix	K48R1	−3.2	94	−1.1
C-terminal	R80R1	−4.5	80	−1.2
	K135R1	−1.8	82	−0.6
loop	D22R1	0	100	0
	G51R1	−2.5	84	−0.8
tertiary	A74R1	0	95	0
interaction	V75R1	−3.2	96	−1.1
	N81R1	−2.9	94	−1
	V87R1	−11	62	−4
	A130R1	−3.1	84	−1
	I150R1	−4.8	85	−1.5
buried	L99R1	−13.3	64	−4.2
	L133R1	−9.5	73	−3.1
	F153R1	−13	57	−4.1
side-chain	(A)65[a]	−2	97	−0.7
variants	(G)65[a]	−4	91	−1.3
	(A)7[2a]	−2.2	91	−0.63

[a] (A)65 and A(72) are K65R1/N68A and D72R1/N68A/R76A, respectively.

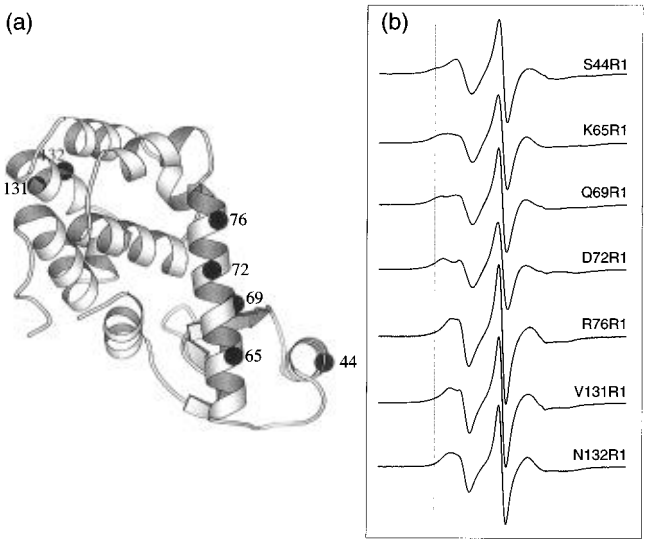

FIGURE 4: (a) Crystal structure of T4L showing the location of helix surface sites. (b) Corresponding EPR spectra of side-chain R1. The magnetic field scan width is 98 G. All T4L structures (this figure and Figures 4, 7, 8, 10−12, and 14) are represented with MOLSCRIPT (Kraulis, 1991).

general not orthogonal, and the spectra may not be accurately fit by models of motion that involve diffusion about mutually perpendicular axes. Simulations employing Brownian dynamic models offer an attractive possibility for future study (Robinson et al., 1992; Altenbach et al., 1994; H.-J. Steinhoff, personal communication). Due to the complexity of the problem, detailed spectral simulations have not yet been attempted to extract dynamic information. For the purposes of this paper, a more qualitative description of the motion will suffice to reveal the relationship between side-chain mobility and protein structure. The term "mobility" will be used in a general sense to include effects of both molecular ordering and motional frequency. Thus a state of low mobility can arise from either a large amplitude of motion with a low frequency or a restricted range of motion with a high frequency. Two crude estimators of mobility can be gleaned from the spectrum without full simulations. These are (1) the overall breadth of the spectrum along the magnetic field axis and (2) the line width of the central ($m_I = 0$) resonance. These criteria will be the basis for qualitative judgments regarding relative mobilities within structural categories and finally employed as semiquantitative measures for drawing conclusions regarding the general relationship between mobility and protein structure.

Mobility of Nitroxide Side Chains at Solvent-Accessible Surfaces of α-Helices. (a) Surface Sites without Tertiary Interaction. The sites in this category (S44R1, K65R1, Q69R1, D72R1, R76R1, V131R1 and N132R1) were selected so that the nitroxide side chains are unlikely to make contact with other parts of the protein, based on the crystal structure (see Figure 4a). As can be seen in Tables 1 and 2, nitroxide substitution at these sites does not result in any measurable changes in activity or stability. Figure 4b shows the EPR spectra. Although the spectra are from topographically equivalent sites, the details of the line shapes reveal quantitative differences in mobility that arise from either interactions with nearest neighbor side chains and/or segmental motions.

To examine the influence of side-chain interactions within a helical structure, nearest neighbor variants of D72R1 and K65R1 in helix C, S44R1 in helix B, and V131R1 in helix H were constructed (Figure 5). Helix B and helix H have been shown to tolerate multiple alanine replacements on their exposed surfaces without any significant structural changes (Zhang et al., 1992; Heinz et al., 1992). Consistent with this, the thermal stabilities of D72R1 variant 1 and D65R1 variants 1 and 3 are only marginally less stable than that of the wild-type protein (Table 2).

The spectrum of D72R1 is characteristic of an anisotropic motion about an axis roughly parallel to the nitroxide 2pπ orbital (Freed, 1976; Seelig, 1976). The nitroxide at this site has one of the most constrained motions of the solvent-exposed helix surface class. Substitution of the bulky $i+4$ R76 residue with alanine has virtually no effect on the mobility of D72R1 (variant 1, Figure 5a). Substitution of the $i-3$, $i\pm4$ residues by alanine (variant 2, Figure 5a) or the $i+3$, $i+4$ residues by alanine (variant 3, Figure 5a) does not alter the anisotropic line shape, which reflects the basic geometry of the motion, but does reduce the spectral breadth as measured by the splitting of the outer hyperfine extrema by about 5 G. This is a relatively small effect compared with the fundamental differences in line shapes observed between the various helix surface sites and may arise from secondary effects on backbone dynamics. This is suggested by the fact that multiple substitutions within $i-3$, $i\pm4$ are required to produce the observed effect, whereas single alanine substitutions at any of the sites do not (data not shown).

The spectrum of D65R1 indicates a more isotropic motion relative to that at D72R1. At this position, there is little effect of alanine substitution at $i\pm4$ (variant 1, Figure 5b) or $i+3$, $i+4$ (variant 2, Figure 5b). Residue $i-3$ was not substituted since it is involved in a hydrogen bond with the helix capping residue threonine 59. Even when the $i\pm4$ residues are replaced with glycine, only a minor effect on line shape is observed (variant 3, Figure 5b).

Panels c and d of Figure 5 show the effect of various substitutions around S44R1 and V131R1 in helices B and H, respectively. The spectrum of S44R1 is complex,

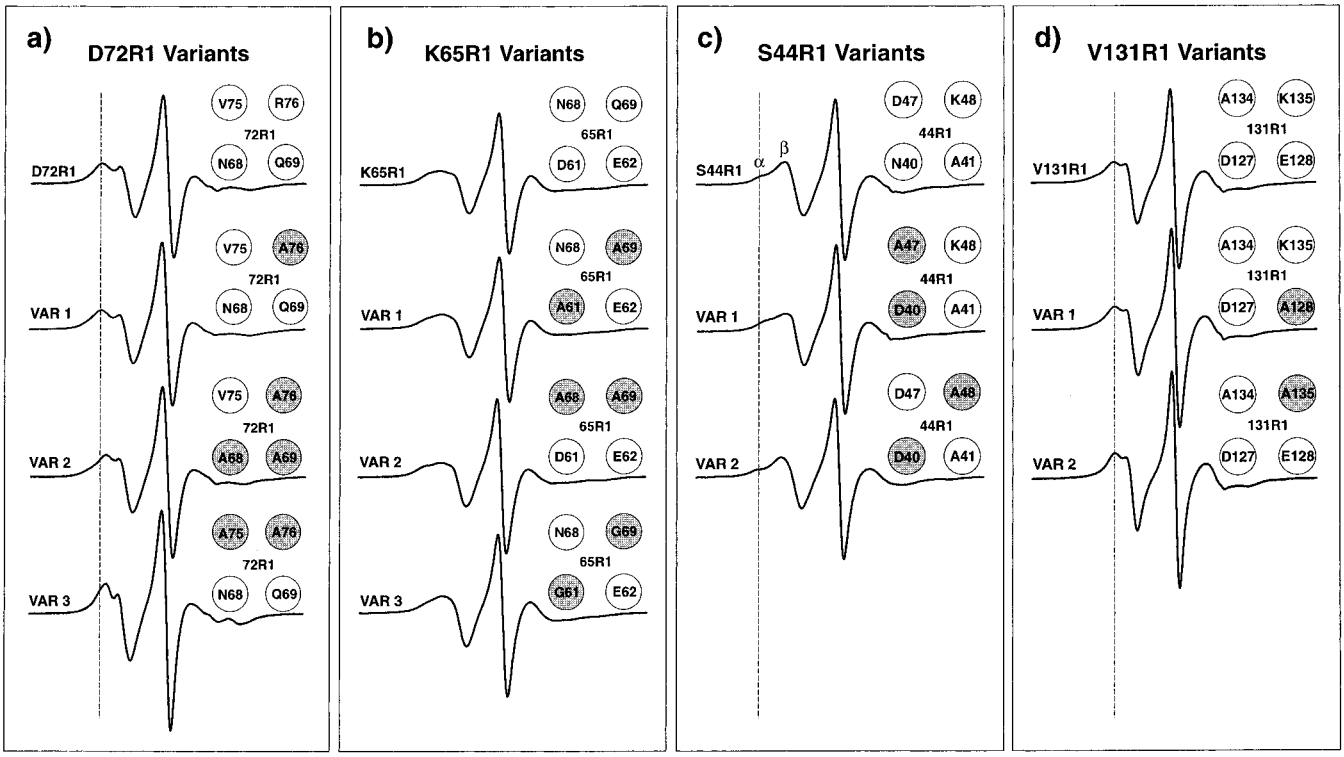

FIGURE 5: Dependence of R1 side-chain mobility on nearest neighbor side chains for helix surface sites. Open and shaded circles represent native and mutated residues, respectively. The vertical dashed lines are provided to aid the eye in comparing the positions of resolved outer resonance peaks. The magnetic field scan width is 98 G.

reflecting two resolved populations of different mobilities (α and β, Figure 5c). This line shape, unlike that of D72R1, could not be simulated from any motional model having a single component. The spectrum of V131R1 can be accounted for by a simple anisotropic motion similar to that of D72R1, but with a larger amplitude of motion of the $2p\pi$ orbital axis (Figure 5d). Variants 1 at the two sites were selected to give identical $i\pm3$, $i\pm4$ residues around the respective nitroxide side chains. As can be seen, the spectra remain distinctly different, each similar to that with the respective wild-type nearest neighbors. In variants 2, the bulky $i+4$ lysine is replaced by alanine. Again, the spectra are essentially identical to those with the respective wild-type nearest neighbors. The above results collectively demonstrate *that the main determinant of the side-chain motion is not steric interaction with nearest neighbors within the helix*. This being the case, the distinctive motion at each site, reflected by the different spectral line shapes for the same spin-labeled side chain, is likely to be dominated by the structure and/or dynamics of the backbone, although we do not exclude the possibility that hydrophobic interactions of the nitroxide ring with the backbone or neighboring side chains may contribute. This conclusion will be further explored in the Discussion.

As mentioned above, the dynamics of a nitroxide side chain is expected to depend on the structure of the nitroxide side chain as well as on the local protein structure. The EPR spectrum of the R1 side chain at position 72 reflects a restricted, anisotropic motion. This is a remarkable result, considering the apparent lack of interaction with nearest neighbor side chains and the existence of multiple bonds in the side chain about which free rotation could potentially occur. Rotation about the $C\alpha-C\beta$ bond is hindered by the interaction of the β-carbon with the backbone of the preceding turn, and rotation about the disulfide is restricted by a high potential barrier ($\geq$7 kcal/mol) (Hubbard et al., 1958; Fraser et al., 1971; Jiao et al., 1992). However, rotations about the $C\beta-S\gamma$, $S-C_\delta$, and $C_\delta-C_\epsilon$ bonds are expected to give rise to a high mobility (Figure 1).

To examine the origin of the motional restriction of R1 at helix surface sites, the mobility of side chains R1, R2, and R3 (Figure 1) at positions 72, 44, and 131 is compared. In contrast to R1, the mobility of R3 is influenced by the bulky arginine and lysine residues at the $i+4$ position. This effect will be analyzed in a future publication. To reduce nearest neighbor side-chain effects and focus on the intrinsic side-chain mobility determined by internal bond rotations, the comparison is made with the $i+4$ arginine and lysine residues replaced by alanine.

Figure 6 shows a comparison of the EPR spectra of V131[R1, R2, R3]/K135A and S44[R1, R2, R3]/K48A. First consider the comparison of R1 with R2. It is immediately apparent from the broad spectral line shapes of R2 at each site that this side chain has an even more restricted mobility than R1, even though the linkages connecting the nitroxide to the backbone are identical. Molecular modeling indicates that the presence of the 4-methyl substituent in R2 effectively prevents rotation about the terminal bond to the nitroxide ring due to steric interactions with the distal sulfur of the disulfide. Thus the motion that averages the nitroxide magnetic interactions in R1 is apparently rotation about the terminal bond in the side chain. Effective rotations about the $C_\beta-S_\gamma$ bond must be largely restricted.

To evaluate the role of the disulfide in restricting rotation about the $C_\beta-S_\gamma$ bond in R1, the side-chain R3 with a thioether linkage was employed. Even though the linkage of R3 contains one less sulfur and one less bond, the EPR spectra of R3 at each site reveal a *greater* mobility than R1. Moreover, the spectra of R3 reflect a single population of spins with essentially isotropic motion, whereas the spectra

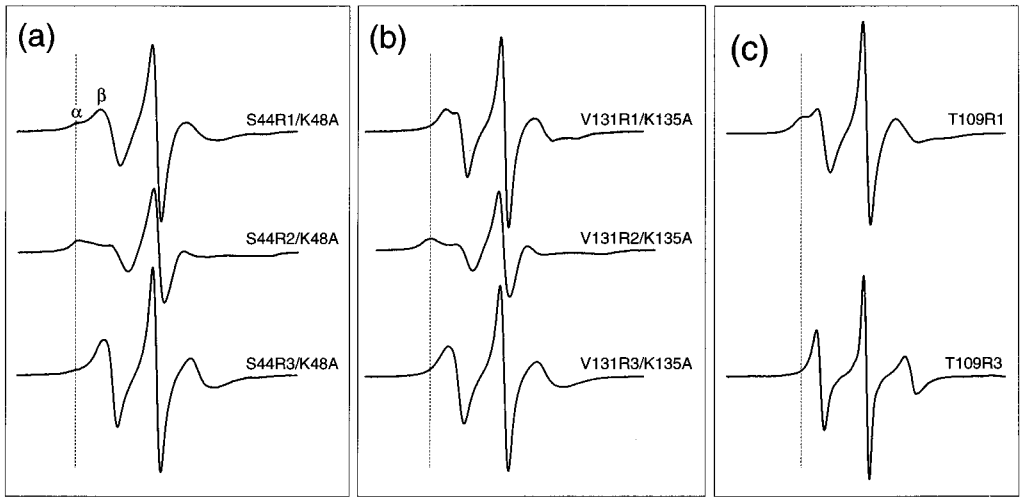

FIGURE 6: Comparison of the EPR spectra of R1, R2, and R3 at (a) S44/K48A, (b) D72/R76A, and (c) T109. The vertical dashed lines are provided to aid the eye in comparing the positions of resolved outer resonance peaks. The magnetic field scan width is 98 G.

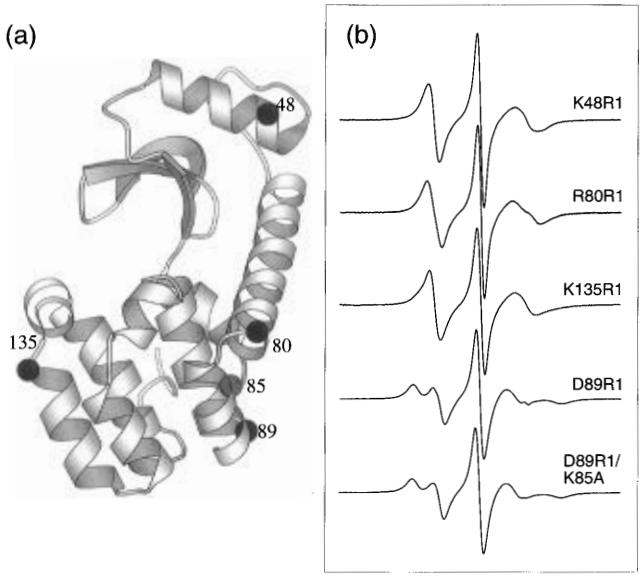

FIGURE 7: (a) Crystal structure of T4L showing the location of helix C-terminal sites (black spheres) and the site of the K85A mutation (gray sphere). (b) Corresponding EPR spectra of side-chain R1. The magnetic field scan width is 98 G.

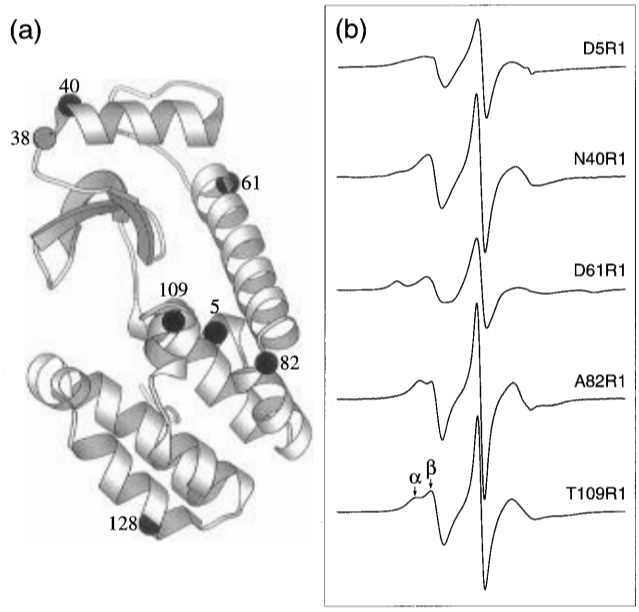

FIGURE 8: (a) Crystal structure of T4L showing the location of helix N-terminal sites (black spheres) and the location of the N-cap, S38 (gray sphere). (b) Corresponding EPR spectra of side-chain R1. The magnetic field scan width is 98 G.

of R1 are either anisotropic or multicomponent. Collectively, the above results point to the disulfide as the origin of the highly restricted and complex motion seen in R1 at internal helix sites. Similar results are found for the spin-labeled side chains R1, R1, and R3 at position 72 (data not shown).

(b) Helix Termini. (1) Helix C-Terminal Residues. C-Terminal sites are those within the last turn of a helix and are represented by K48R1, R80R1, and K135R1 (see Figure 7a). These are solvent-exposed sites whose side chains are not expected to have tertiary contacts or other interactions. D89R1 is a special case that will be discussed separately. The EPR spectra of the C-terminal sites K48R1, R80R1, and K135R1 are striking in their exceptionally high mobility (Figure 7b). Since the absence of neighboring side chains at $i\pm4$ is not expected to dramatically alter the mobility at these sites, it is likely that the relatively mobile spectrum observed is due to thermal fluctuations in the backbone around these regions.

To examine the role of backbone flexibility in determining mobility at the C-terminal sites, D89R1 was constructed. D89 is near the C-cap of helix D, but the backbone has a low crystallographic thermal factor, apparently arising from a stabilizing interaction of the carbonyl oxygen of D89 with the ϵ-amino group of R96 (Weaver et al., 1989; Tidor & Karplus, 1991). The EPR spectrum of D89R1 reflects a highly restricted motion, similar to that observed at D72R1, consistent with the low thermal factor. To test whether the effect is due to an unusual side-chain interaction with the nearby bulky side chain of K85, D89R1/K85A was constructed (Figure 7a). As shown in Figure 7b, the spectrum of this mutant is very similar to that of D89R1, supporting the conclusion that a rigid backbone can stabilize an ordered conformation of R1.

(2) Helix N-Terminal Residues. N-Terminal residues are defined as sites located within a helix at the N1, N2, or N3 positions (Nicholson et al., 1991). In this category are E5R1, N40R1, D61R1, A82R1, and T109R1, all located in the first turn of their respective helices, fully solvent exposed, and without significant tertiary interactions (Figure 8a). In sharp constrast to the C-terminal residues (other than D89R1), the EPR spectra of these sites reflect relatively restricted mobility

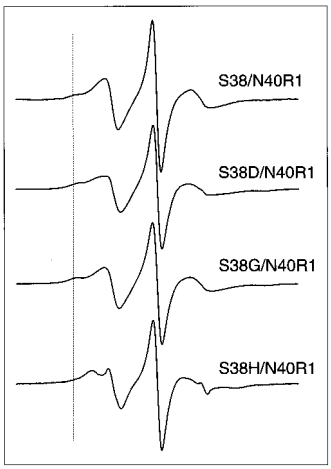

FIGURE 9: Effect of mutating the N-terminal capping residue, S38, on the mobility of side-chain R1 at site N40. The vertical dashed line is provided to aid the eye in comparing the positions of resolved outer resonance peaks. The magnetic field scan width is 98 G.

with multiple components, one of which is relatively immobilized, or anisotropic (Figure 8b). In general, these spectra are more similar to those at helix surface sites (Figure 4b). The EPR spectrum of R3 at T109 shows a complete absence of the motionally restricted component (Figure 6c), offering further support for the conclusion that the interaction of the disulfide with the backbone is the origin of the complex spectrum of R1 at exposed sites.

To further investigate the origin of the striking difference between the N- and C-terminal sites, particularly with regard to the existence of a relatively immobilized component, mutants of N40R1 with the capping residue S38 replaced by glycine, aspartate, or histidine were prepared. Serine aspartate and glycine are considered to be effective N-caps as they stabilize helices when introduced at this position (Harper & Rose, 1993; Harpaz et al., 1994). On the other hand, histidine is a poor capping residue. As shown in Figure 9, the EPR spectra of N40R1, N40R1/S38G, and N40R1/S38D are very similar in basic line shape, having two well-resolved components, while that for N40R1/S38H has a distinctive line shape characteristic of an anisotropic motion of the nitroxide in which the immobilized component has disappeared. The extent of the spectral change on substitution of the N-capping residue S38 for histidine exceeds that resulting from nearest neighbor interactions and provides direct evidence for the role of the N-cap residue in stabilizing the more immobilized state of the nitroxide side chain at N40R1. This effect could result from a dynamic "fraying" of the N-terminal region in the absence of an effective N-cap residue. The variant S38H of mutant S44R1 does not show any change in the EPR spectrum (data not shown), consistent with a specific interaction between R1 and the N-cap region.

Mobility of Nitroxide Side Chains in Loops. Loop sites are in sequences connecting regular secondary structural elements and are represented here by D22R1, K35R1, and G51R1 (see Figure 10a). All three residues are solvent exposed and are in regions of the protein characterized by a high crystallographic thermal factor (Alber et al., 1987). The EPR spectra shown in Figure 10b indicate that the nitroxides are all of high mobility, similar to those of the C-terminal sites. The increased mobility relative to internal helix sites can arise from a decrease in steric constraints imposed on nanosecond rotation about the Cα−Cβ bond in a helix, a

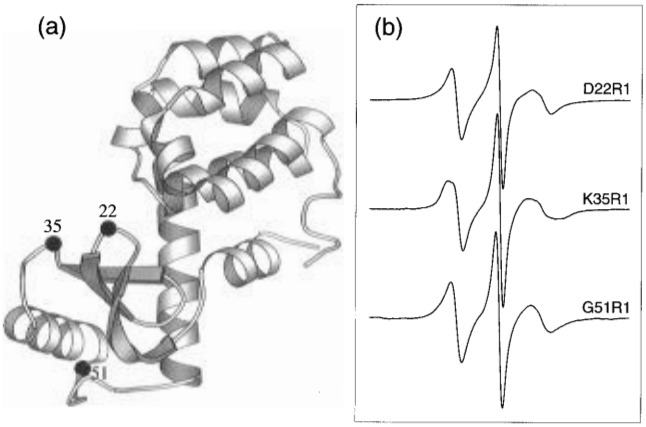

FIGURE 10: (a) Crystal structure of T4L showing the location of loop sites. (b) Corresponding EPR spectra of side-chain R1. The magnetic field scan width is 98 G.

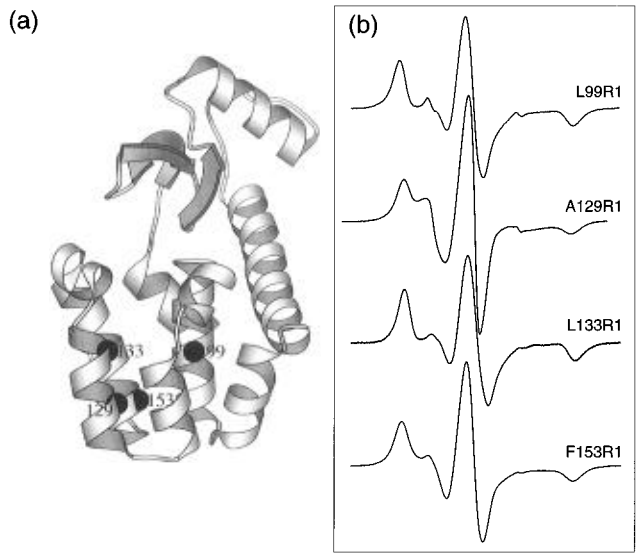

FIGURE 11: (a) Crystal structure of T4L showing the location of buried sites. (b) Corresponding EPR spectra of side-chain R1. The magnetic field scan width is 98 G.

large amplitude of motion of the backbone in the nanosecond regime, or a combination of both. To resolve the contribution of the two factors, compare the EPR spectrum of K48R1 (Figure 7) to that of G51R1. K48R1 is at the C-cap +2 position of helix B, while G51R1 is located in a loop. Despite the dramatic difference in their neighboring side-chain molar volumes and the steric constraints imposed on the Cα−Cβ rotation, the two sites have very similar spectra. This suggests that the major determinant of the mobility at these sites is backbone flexibility.

Mobility of Nitroxide Side Chains at Buried Sites. Buried sites are those with no solvent accessibility and are represented by L99R1, A129R1, L133R1, and F153R1 (Figure 11a). These sites are located within the compact hydrophobic core of the C-terminal domain of T4L and have an almost isotropic distribution of main-chain atoms around them. The tight packing of the protein interior is expected to allow little, if any, motion of the nitroxide side chain relative to the protein. The EPR spectra (Figure 11b) are consistent with this expectation and have "powder" line shapes characteristic of nitroxides in the slow motional regime. In fact, the rotational correlation time of L99R1 and L133R1 computed from the splitting of the outer hyperfine extrema is ap-

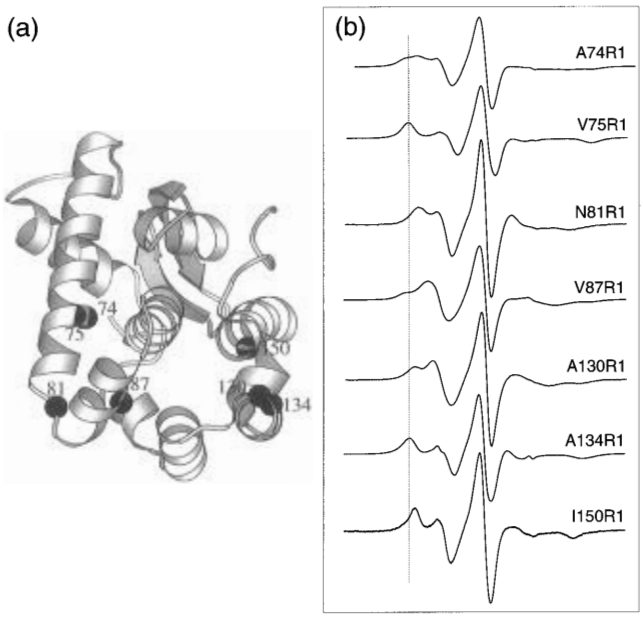

FIGURE 12: (a) Crystal structure of T4L showing the location of tertiary contact sites. (b) Corresponding EPR spectra of side-chain R1. The vertical dashed line is provided to aid the eye in comparing the positions of resolved outer resonance peaks. The magnetic field scan width is 98 G.

proximately 20 ns (Freed, 1976), consistent with the rotational motion of the protein as a whole in 30% sucrose. That the residual motion of these nitroxides is due to protein rotation is further supported by the linear dependence of the effective correlation time on viscosity in solutions of different sucrose concentrations (data not shown).

Thus the dynamic properties of these side chains inferred from the EPR spectra are fully consistent with the overall three-dimensional fold of the protein, even though these buried mutants suffer considerable thermodynamic destabilization (Table 2). In further support of a native-like fold for these mutants are the circular dichroism spectra which closely resemble that of the wild-type protein (Figure 2) and the absence of a measurable collision rate of the nitroxide with the paramagnetic reagent NiEDDA in solution, indicating solvent-inaccessible sites.

Mobility of Nitroxide Side Chains at Tertiary Interaction Sites. Tertiary interaction sites are defined as sites where substitution with R1 creates steric conflicts with proximal side-chain and main-chain atoms. However, unlike buried sites, the distribution of atoms in contact with the nitroxide is not isotropic. This is by far the most heterogeneous class with respect to side-chain mobility, because both degree of tertiary interaction and backbone dynamics vary from site to site. The backbone flexibility determines local repacking as a result of amino acid substitution (Baldwin et al., 1993). Therefore, it is expected to influence the degree of order of the side-chain R1. Mutants A74R1, V75R1, N81R1,V87R1, A130R1, A134R1, and I150R1 represent this class (Figure 12a). The EPR spectra (Figure 12b) reveal distinctive multicomponent features (A130R1, A74R1, V87R1), highly anisotropic motion (I150R1), or near immobilization (A134R1, V75R1), each arising from the structural constraints imposed on the mobility by the interaction.

To fully appreciate the unique aspects of the spectra arising from the interaction, they should be compared with those of nearby sites in the same helix that are expected to have approximately the same backbone dynamics but belong to a different structural class. For example, tertiary interaction site A130R1 lies between the adjacent buried residue 129 (Figure 11) and surface site 131 (Figure 4) in terms of mobility, consistent with the expected tertiary interaction. A similar conclusion applies to residue A134R1 located between buried residue 133 (Figure 11) and C-terminal site 135 (Figure 7). In the latter case, the nitroxide has very low, but significantly greater mobility than the adjacent buried residue L133R1, as judged by the central line width and the separation of the outer hyperfine extrema. This is entirely consistent with the structure, which shows that the 133 side chain makes more contacts with nearby atoms than 134.

Another comparison between tertiary interaction sites that are expected to have similar backbone dynamics is provided by A130R1 and I150R1 (Figure 12b). They are predicted to have different degrees of tertiary interaction, as judged from the orientation of the side chains with respect to their respective helical axes. However, they both lie on the same interface between helices H and I and are in regions of similar crystallographic thermal factors. The relative mobilities of the nitroxide, clearly reflected in the separation between the outer hyperine extrema, are consistent with the predicted increased interactions between the nitroxide and neighboring side-chain and main-chain atoms at site I150R1.

The degree of tertiary interaction revealed in the EPR spectrum appears to be modulated by the flexibility of the backbone. This is illustrated by site N81R1. This site is in a flexible region of the protein, near the putative hinge-bending locus (Dixon et al., 1992). The mobility measured by the separation of the outer hyperfine extrema is not significantly different than those observed for exposed sites on the outer surfaces of helices (such as D72R1). Thus a degeneracy can arise in attempting to distinquish tertiary interaction sites from exposed sites on rigid helices using mobility criteria alone. This degeneracy can be resolved by using the $i\pm1$ residue as a reference to sample the local backbone dynamics. For example, if the neighboring residue to a relatively immobilized side chain is mobile, then it is probable that the residue in question is in tertiary contact. In future publications, we will show that such degeneracies can also be resolved with the application of nitroxide side chains with different structures.

DISCUSSION

The primary objectives of this work were to (1) evaluate the degree of perturbation of the R1 side chain with respect to enzymatic activity, secondary structure, and thermal stability and (2) to explore the relationship between the mobility of the R1 side chain and protein structure. Below we discuss the results relative to these objectives.

Perturbation Due to the Nitroxide Side Chain. T4L was selected as the object for study because of the exhaustive mutagenesis and structural analysis reported in the literature. The present work extends the mutagenesis to include a non-native side chain, R1. The effects on enzymatic activity (Table 1) and thermal stability (Table 2) due to substitution with R1 at the various sites generally reflect the conclusions drawn by Matthews and co-workers for substitution with native amino acids at the same or similar sites (Alber et al., 1987). Thus for solvent-exposed helix surface sites, sub-

stitution by R1 produces little change in activity or thermal stability, except at N132 where the original residue is involved in substrate binding (Shoichet et al., 1995). At this site there is a 40% reduction in activity, although the thermal stability is *increased*, consistent with earlier findings with substitutions with Met, Phe, or Ile. Among the solvent-exposed helix sites, only those at or near the C-termini showed a measurable destabilization (≈−1 kcal/mol) and/or a reduction in activity upon substitution with R1. Similar effects were observed at these sites upon substitution with natural amino acids (Lu et al., 1992; Matthews, 1995). Substitutions at the loop sites were essentially without effect. Thus we assume that information obtained from the EPR spectra of R1 at solvent-exposed sites generally reflects the native structure.

As expected, substitutions for R1 at buried sites L99, L133, F153, and A129 produced the greatest loss of activity and thermal destabilization. Rearrangements of the core are clearly needed to accommodate the increased volume of R1. Despite the destabilizations, the mutants show reversible thermal unfolding and have CD spectra similar to that of the wild type. Moreover, the R1 side chains are inaccessible to collision with the polar reagent NiEDDA, consistent with a folded structure. To understand the nature and extent of structural rearrangements will require crystallographic structure determination. However, it is instructive to compare the thermodynamic stability of these mutants to those reported in the literature. Matthews and co-workers (Eriksson et al., 1993) have constructed mutants at these same sites: L99A ($\Delta\Delta G = -5$ kcal/mol; compare with −4.2 for L99R1), L133A ($\Delta\Delta G = -3.6$ kcal/mol; compare with −3.1 for L133R1), and F153A ($\Delta\Delta G = -3.5$ kcal/mol; compare with −4.1 for F153R1). It is remarkable that substitution for alanine produces very similar destabilizations as R1 at the same sites, although undoubtedly the result of very different repacking effects. Despite the large destabilizations, the X-ray structures of the alanine mutants revealed only subtle structural rearrangements on the level of the backbone fold that involved the movement of main-chain atoms to repack the core. It is believed that such movements have a large contribution to the change in stability and tend to propagate the structural alteration to sites relatively distant from the mutation site. This in turn leads to the sharp reduction in biological activity observed for this class of mutants.

Although the tertiary interaction sites investigated are nearly solvent inaccessible, we have chosen to classify them as a separate category for two reasons. First, the local topography is such that the R1 side chain can avoid steric clashes with nearby main-chain atoms by assuming alternative conformations, unlike the case for buried residues. This property leads to significantly less destabilization as compared to buried sites (see Table 2). Only V87R1 shows significant destabilization. Second, the conformations of the R1 side chain adopted to relieve steric interactions lead to a characteristic EPR spectrum distinct from the buried sites. Matthews and co-workers (Blaber et al., 1993) have examined changes in thermal stability in mutants at some of the same sites examined here: V75T ($\Delta\Delta G = -1.3$ kcal/mol; compare with V75R1 = −1.1), V87T ($\Delta\Delta G = -1.0$ kcal/mol; compare with V87R1 = −3.95), and A130S ($\Delta\Delta G = -0.7$ kcal/mol; compare with −1.0 for A130R1). Only V87R1 is significantly more destabilized than threonine or serine substitution mutants at equivalent sites. The structure of the serine/threonine mutants differed from the wild type only in side-chain conformations, well below the level of resolution sought in the spin-labeling experiment.

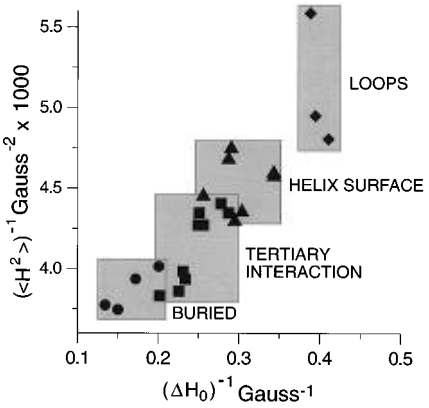

FIGURE 13: Reciprocal second moment versus the reciprocal central line width calculated from the EPR spectra of R1 at the sites shown.

General Correspondence between Structure and Side-Chain Mobility. In the Results, relative R1 mobility was presented in qualitative terms for each of the topographical classes defined. To provide an overview of the global relationship between structure and mobility, it is convenient to identify semiempirical measures of mobility derived from the EPR spectra. The peak-to-peak first derivative width of the central ($m_I = 0$) resonance (ΔH_o) and the spectral breadth are two such measures, the latter of which can be represented by the spectral second moment ($\langle H^2 \rangle$) (Slichter, 1992). The numerical value of these quantitites at X-band frequencies is determined primarily by the degree of averaging of the anisotropic **g** tensor and the anisotropic hyperfine tensor, respectively. As the frequency of nitroxide rotational motion is reduced, the second moment and line width always increase for any particular motional geometry. The same is true for increases in molecular ordering about any particular axis. Thus the second moment and line width are functions of both rate and order of motion and may be used as simple measures of mobility in the general sense for a particular nitroxide side-chain structure. These quantitites cannot be used, however, to quantitatively compare mobility between nitroxide side chains of different structures that might have, for example, anisotropic motions about different axes. For sites at which multiple populations of mobility states are observed, the central line width, measured from the first derivative spectrum, will be dominated by the most mobile component unless it is present in extremely small amounts. On the other hand, the second moment will be biased toward the immobilized component. The price paid for use of these simple measures of mobility is that much information on side-chain motion is lost. For example, specific features of motional anisotropy and the existence of multiple side-chain conformations are lost. Nevertheless, they permit the presentation of a large amount of data in a manner that reveals the general relationship between structure and line shape.

In order that the measures be increasing functions of mobility, the reciprocal of these quantities will be employed. Figure 13 shows a plot of the reciprocal second moment versus the reciprocal central line width for the spectra of R1 side chains representing helix surface, loop, tertiary interaction sites, and buried sites. The points for C- and N-terminal

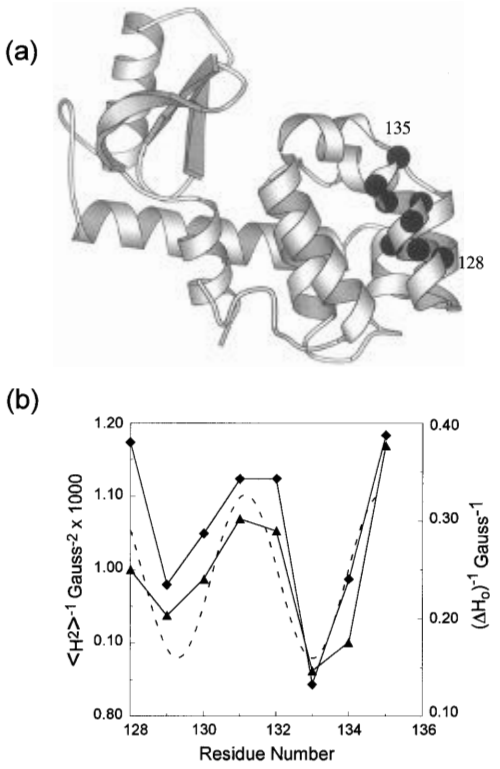

FIGURE 14: R1 scanning through helix H in the C-terminal domain of T4L. (a) Crystal structure of T4L showing the topographical location of the scanning sites. (b) Mobility parameters calculated from the EPR spectra of each site. (▲) represents $\langle H^2\rangle^{-1}$ and (♦) represents $(H_o)^{-1}$. The dashed line represents a function with a period 3.6.

sites have not been included for simplicity. In most cases, these points would overlap the loop and helix surface domains, respectively.

As is apparent in Figure 13, points for R1 side chains in a given structural class are clustered together in mobility, and the mobilities are consistent with that expected from the tertiary fold of T4L. Thus buried sites are all located in the low-mobility region of the plot, as expected for the densely packed interior of the protein. Tertiary interaction sites have a mobility intermediate between helix surface sites and buried sites, and loop sites have the highest mobility. There are overlaps among the areas representing buried and tertiary interaction sites and between tertiary interaction sites and helix surface sites. These overlaps result, in part, from effects of backbone dynamics superposed on the effects of tertiary interactions. In future work, means of resolving this degeneracy based on the use of different nitroxide side chains will be presented.

As an illustration of $(\Delta H_o)^{-1}$ and $(<H^2>)^{-1}$ as measures of mobility, consider the sequential substitution of R1 through the complete helical segment from 128 to 135. Figure 14a shows the locations of the sites in the T4L molecule. The spectra corresponding to this "R1 scan" can be found in the appropriate figures above. Figure 14b shows a plot of both $(\Delta H_o)^{-1}$ and $(\langle H^2\rangle)^{-1}$ versus amino acid number that clearly reveals the expected periodicity in mobility associated with the α-helix. In summary, the data in Figures 13 and 14 indicate that *the mobilities of the side chains reflect the fold of the protein deduced from the crystal structure.*

Determinants of the Mobility of the R1 Side Chain in T4L. The low mobility of the R1 side chain with respect to the protein at the buried sites is readily rationalized in terms of steric interactions of the nitroxide within the densely packed core of the protein and the low crystallographic thermal factors at these sites (Albers et al., 1987).

The high isotropic mobility of R1 at solvent-exposed loop sites can be understood primarily on the basis of backbone dynamics, reflected by the high thermal factors at these sites, although the increased freedom of rotation about the $C_\alpha-C_\beta$ bond in loops compared to sites in helical structures may contribute. The amplitude of backbone fluctuations necessary to account for the spectral line shapes will have to be determined by spectral simulation, but it can be concluded that the effective correlation time must lie in the nanosecond range or faster.

Similarly, the mobility of R1 at the solvent-exposed C-terminal sites can be accounted for by backbone thermal fluctuations. Thus, the high and low mobilities of R80R1 and D89R1 correlate with high and low thermal factors at those sites, respectively. In the latter case, the mobility is dominated by internal bond rotations in the side chain (see below). Comparison of side-chain mobility with the crystallographic thermal factors at K48R1 and K135R1 is complicated by the existence of crystal contacts at these sites which act to dampen backbone and side-chain motions (Weaver & Matthews, 1987; Zhang et al., 1995). However, molecular dynamics simulations for the solution structure suggest that these regions have considerable backbone motions (Arnold & Ornstein, 1992), consistent with the high mobility of R1 observed at these sites.

The complex multicomponent or anisotropic EPR line shapes observed at tertiary interaction sites can be rationalized on the basis of the expected steric interactions with nearby atoms in the structure. To resolve two components in the EPR spectrum differing in resonance position by ≈10 G, as observed for A130R1, A74R1, and V87R1 (Figure 12b), the exchange rate between the populations must have an activation barrier of ≈7 kcal or greater. Barriers of this magnitude can arise from rotation about the disulfide of the spin-labeled side chain or interactions with the protein that require protein movement for interconversion of states, as observed earlier in spin-labeled hemoglobin (Moffat, 1971).

The origin of the relatively restricted mobility of R1 at sites on the solvent-exposed surfaces of α-helices and at N-terminal sites is of some interest because interactions with nearest neighbor side chains are weak (Figure 5) and tertiary interactions are absent (Figures 4b and 8b). As shown in Figure 6, replacement of the disulfide in the R1 side chain by a thioether linkage (R3) results in a state of high mobility at both helix surface and N-terminal sites. This important result indicates that the restricted mobility has its origin in the disulfide bond and not simply in backbone dynamics. Moreover, the restricted mobility is not due to the hindered rotation about the disulfide, but must arise from immobilization of the disulfide itself, presumably by interaction with the protein backbone. This conclusion is supported by the fact that the 4-methyl derivative of R1 (R2) is highly immobilized (Figure 6), apparently from hindered rotation about the terminal $C_\delta-C_\epsilon$ bond (Figure 1). This implies that the dominant motion leading to averaging of the magnetic parameters of the nitroxide is rotation about this bond and that the entire segment $[-C_\alpha-C_\beta-S_\gamma\text{-}S-]$ is immobile on the EPR time scale.

The observed anistropic EPR spectra at several helix surface sites (Figure 4b) are entirely consistent with this

simple picture. Examination of molecular models of an energy-minimized R1 side chain indicates that restricted rotations about the $C_\delta-C_\epsilon$ and $S-C_\delta$ bonds result in an anisotropic motion that moves the $2p\pi$ orbital axis of the nitroxide within a limited cone. Such *z*-axis anisotropic motions in an isotropic distribution have been extensively investigated with both effective Hamiltonians (Hubbell & McConnell, 1971; Van et al., 1974; Timofeev & Samarianov, 1993) and microscopic order−microscopic disorder (MOMD) models (Meirovitch et al., 1984; Ge & Freed, 1983) and give rise to unique spectral line shapes similar to those of D72R1, R76R1, V131R1, and N132R1. The differences between these spectra can be accounted for by differences in amplitudes of motion of the $2p\pi$ orbital arising from additional degrees of freedom from backbone fluctuations. The thermal factors at 76, 131, and 132 are all larger than at 72, consistent with a larger amplitude of motion of the nitroxide at the former sites.

The spectral line shapes at helix surface sites S44 and N69 are more complex, suggesting two spin populations resolved by roughly 10 G in magnetic field. Resolution of these two populations implies and activation barrier for interconversion between the populations of at least 7 kcal/mol. It is unlikely that such a large activation barrier could arise from simple attractive interactions of the nitroxide spin-label with the protein but could be due to the high rotational barrier about the disulfide. The reason why the two disulfide isomers would be observed at these sites but not at other topographically equivalent sites is not clear. However, an interaction of the disulfide with the backbone may depend on details of the backbone structure and dynamics, which differ significantly from site to site.

The above results suggest an immobilization of the disulfide and proximal bonds through interaction of the disulfide group with the protein. Although specific models for the putative interaction remain to be elucidated, it is reasonable to propose that for solvent-exposed helix surface sites the disulfide is adsorbed to the helix backbone by hydrophobic and/or van der Waals interaction. Configurations of the R1 side chain that place the disulfide in van der Waals contact with backbone atoms have a low configurational internal energy based on calculations using the Biosym CVFF force field (see Figure 15a). An interaction of this type can account for the lack of nearest neighbor side-chain interactions with R1 on a helix surface, because the nitroxide is constrained to a relatively small volume.

A more specific interaction for the disulfide with the protein backbone may be suggested for the motionally restricted N-terminal sites. The literature contains a number of examples where the S sulfur in a disulfide bond appears to form hydrogen bonds with backbone amides. In a survey of high-resolution structure, 32% of sulfurs in a disulfide were found within 4 Å of a hydroxyl oxygen or a nitrogen atom (Gregoret et al., 1991). For example, in thioredoxin, the active site cysteine 32 forms a disulfide bond with Cys 35. The sulfur atom of Cys 32 appears to form a hydrogen bond with the NH of Cys 35 (Katti et al., 1990). Contacts between the lone pair of electrons on the sulfur and the hydrogen atom of amides have been observed in crystals of penicillamine disulfide (Rosenfield & Parthasarathy, 1975). Such an interaction can account for the striking differences between N-terminal and C-terminal sites, because the disulfide of R1 may form a hydrogen bond with an amide nitrogen whose hydrogen bond potential is not satisfied in the first helical turn, whereas this interaction is not available at C-terminal sites (see Figure 15b).

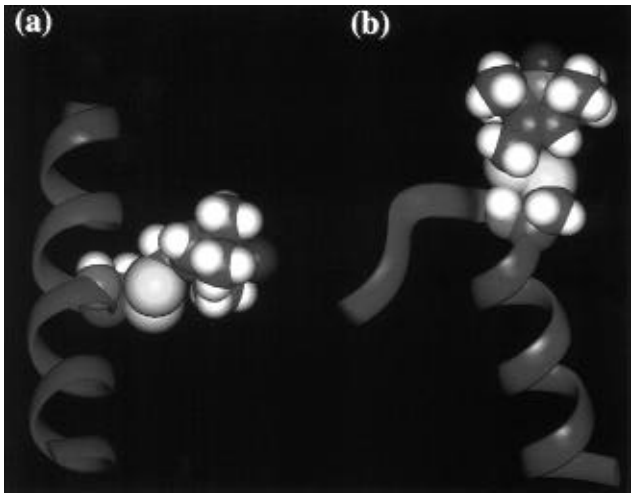

FIGURE 15: (a) Molecular model of side-chain R1 on a helix surface site showing the proximity of the disulfide to the helix backbone. (b) Molecular model of side-chain R1 at an N-terminal site showing potential H-bond formation with a backbone NH.

General Conclusions and Summary. The overall conclusion of the work presented here is that the sequence-dependent variation in the EPR line shape of side-chain R1 provides a fingerprint of the protein tertiary fold that is entirely consistent with expectations based on the crystal structure of the protein. This indicates that the level of structural perturbation due to the R1 side chain is small at the level of the backbone fold and is in accord with the fact that the majority of the spin-labeled mutants show only minor changes in activity or thermal stability and little, if any, alteration in CD spectra. Even for buried site mutants that have relatively large thermal destabilizations, the room temperature EPR spectra are as expected from the structure in each case and clearly show the sites to be immobilized within the hydrophobic core of a folded structure. This is particularly stricking for residues such as 129 and 133 that reside on the nonpolar face of a short (two-turn) helix on the surface of the protein. Here, the periodic variation of the spectral properties unequivocally establishes the existence of the regular helix in the spin-labeled protein. These findings are similar to those of Matthews and co-workers, where substitution of buried site residues produced large thermal destabilizations but relatively small structural changes at the level of the backbone fold. The apparent acceptance of the R1 side chain at buried sites is likely related to its relatively small size, its conformational flexibility, and inherent hydrophobicity. If so, the more traditional sulfhydryl spin-labels such as iodoacetamide and maleimide derivatives may be far less satisfactory.

The mobility of the R1 side chain in proteins is apparently dominated by tertiary interactions and internal backbone dynamics. The R1 side chain has a relatively unique class of spectral line shapes that identify tertiary interactions. Thus, SDSL is a powerful means of mapping tertiary contact sites in proteins of unknown structure. These are valuable data to evaluate computationally generated models for the folds of the protein.

In addition to tertiary contact interactions, the spectra are clearly modulated by internal fluctuations of the backbone.

Assignment of line-shape features to this source may be difficult or ambiguous in the case of tertiary interactions or at buried sites but may be made with some confidence at exposed sites. Since the perturbation due to the R1 side chain is minimal at such sites, SDSL may prove to be a valuable approach to investigate backbone dynamics in both solution and membrane proteins.

Rearrangements of protein tertiary structure and changes in backbone dynamics are involved in the functional mechanism of many proteins as well as in the interconversion of intermediate states on protein folding pathways. The EPR spectra of R1 at tertiary interaction sites are expected to be extremely sensitive to *changes* in the relative positions of the secondary structures involved in the tertiary contact. This sensistivity provides an important approach to the detection of conformational changes in proteins that involve motion of secondary structures, such as rigid body motions of helices. The changes can be monitored in real time in the millisecond range with conventional EPR spectrometers (Farabakash et al., 1993; Steinhoff et al., 1994). Similarly, changes in backbone dynamics can be followed in real time.

The work presented in this paper establishes the basis for interpretation of EPR line-shape changes in terms of structure and sets the stage for application of SDSL to problems such as the solution structure of proteins, time-resolved structure changes along protein folding pathways, and time-resolved detection of functionally related conformational changes.

ACKNOWLEDGMENT

We thank Celia J. Fang for preparation of some of the mutants and Christian Altenbach and Dave Farrens for helpful discussions and careful reading of the manuscript.

REFERENCES

Alber, T., Dao-pin, S., Nye, J. A., Muchmore, D. C., & Matthews, B. W. (1987) *Biochemistry 26*, 3754−3758.
Altenbach, C., Flitsch, S. L., Khorana, H. G., & Hubbell, W. L. (1989) *Biochemistry 28*, 7806−7812.
Altenbach, C., Marti, T., Khorana, H. G., & Hubbell, W. L. (1990) *Science 248*, 1088−1092.
Altenbach, C., Steinhoff, H.-J., Greenhalgh, D., Khorana, H. G. and Hubbell, W. L. (1994) *Biophys. J. 65*, A40.
Arnold, G. E., & Ornstein, R. L. (1992) *Protein Eng. 5*, 703−714.
Baldwin, E. P., Hajiseyedjavadi, O., Baase, W. A., & Matthews, B. W. (1993) *Science 262*, 1715−1718.
Becktel, W. J., & Baase, W. (1985) *Anal. Biochem. 150*, 258−263.
Becktel, W. J., & Schellman, J. A. (1987) *Biopolymers 26*, 1859−1877.
Berliner, L. J., Grunwald, J., Hankovszky, H. O., & Hideg, K. (1982) *Anal. Biochem. 119*, 450−453.
Blaber, M., Lindstrom, J. D., Gasner, N., Xu, J., Heinz, D. W., & Matthews, B. W. (1993) *Biochemistry 32*, 11363−11373.
Blaber, M., Zhang, X.-J., Lindstrom, J. C., Pepiot, S. D., Baase, W. A., & Matthews, B. W. (1994) *J. Mol. Biol 235*, 600−624.
Chothia, C., & Finkelstein, A. V. (1990) *Annu. Rev. Biochem. 59*, 1007−1039.
Dao-pin, S., Anderson, D. E., Baase, W. A., Dahlquist, F. W., & Matthews, B. W. (1991) *Biochemistry 30*, 11521−11529.
Eriksson, A. E., Baase, W. A., & Matthews, B. W. (1993) *J. Mol. Biol. 229*, 747−769.
Farahbakhsh, Z. T., Hideg, K., & Hubbell, W. L. (1993) *Science 262*, 1416−1419.
Fraser, R. R., Boussard, G., Saunders, J. K., & Lambert, J. B. (1971) *J. Am. Chem. Soc. 93*, 3822−3823.
Freed, J. H. (1976) in *Spin Labeling Theory andd Applications* (Berliner, L. J., Ed.) pp 53−161, Academic Press, New York.
Hankovsky, H. O., Hideg, K., & Lex, L. (1980) *Synthesis*, 914−916.
Harpaz, Y., Elmasry, N., Fersht, A. R., & Henrick, K. (1994) *Proc. Natl. Acad. Sci. U.S.A. 91*, 311−315.
Harper, E. T., & Rose, G. D. (1993) *Biochemistry 32*, 7605−7609.
Heinz, D. W., Baase, W. A., & Matthews, B. W. (1992) *Proc. Natl. Acad. Sci. U.S.A. 89*, 3751−3755.
Ho, S. N., Hunt, H. D., Horton, R. M. Pullen, J. K., & Pease, L. R. (1989) *Gene 77*, 51−59.
Hubbard, W. N., Douslin, D. R., McCullough, J. P., Scott, D. W., Todd, S. S., Messerly, J. F., Hossenlopp, I. A., George, A., & Waddington, G. (1958) *J. Am. Chem. Soc. 80*, 3547−3554.
Hubbell, W. L., & McConnell, H. M. (1971) *J. Am. Chem. Soc. 93*, 314−326.
Hubbell, W. L., & Altenbach, C. (1994) *Curr. Opin. Struct. Biol. 4*, 566−573.
Hubbell, W. L., Froncisz, W., & Hyde, J. S. (1987) *Rev. Sci. Instrum. 58*, 1879−1886.
Hurley, J. H., Baase, W. A., & Matthews, B. W. (1992) *J. Mol. Biol. 224*, 1143−1159.
Jiao, D., Barfield, M., Combariza, J. E., & Hruby, V. J. (1992) *J. Am. Chem. Soc. 114*, 3639−3643.
Katti, S. K., & LeMaster, D. M. (1990) *J. Mol. Biol. 212*, 167−184.
Kraulis, P. J. (1991) *J. Appl. Crystallogr. 24*, 946−950.
Lim, W. A., Farruggio, D. C., & Sauer, R. T. (1992) *Biochemistry 31*, 4324−4333.
Lu, J., Baase, W. A., Muchmore, D. C., & Dahlquist, F. W. (1992) *Biochemistry 31*, 7765−7772.
Matsumara, M., & Matthews, B. W. (1989) *Science 243*, 792−794.
Matthews, B. W. (1993) *Annu. Rev. Biochem. 62*, 139−160.
Matthews, B. W. (1995) *Adv. Protein Chem. 46*, 249−278.
Meirovitch, E., Nayeem, A., & Freed, J. H. (1984) *J. Phys. Chem. 88*, 3454−3465.
Moffat, J. K. (1971) *J. Mol. Biol. 55*, 135−145.
Nicholson, H., Anderson, D. E., Dao-pin, S., & Matthews, B. W. (1991) *Biochemistry 30*, 9816−9828.
Robinson, B. H., Slutsky, L. J., & Auteri, F. P. (1992) *J. Chem. Phys. 96*, 2609−2616.
Rosenfield, R. E. J., & Parthasarathy, R. (1975) *Acta Crystallogr., Sect. B 31*, 462−468.
Sauer, U. H., Dao-pin, S., & Matthews, B. W. (1992) *J. Biol. Chem. 267*, 2393−2399.
Seelig, J. (1976) in *Spin Labeling Theory and Applications* (Berliner, I. J., Ed.) pp 373−407, Academic Press, New York.
Shoichet, B. K., Baase, W. A., Kuroki, R., & Matthews, B. W. (1995) *Proc. Natl. Acad. Sci. U.S.A. 92*, 452−456.
Slichter, C. P. (1992) *Principles of Magnetic Resonance*, p 72, Springer-Verlag, Berlin.
Steinhoff, H., Mollaaghababa, R., Altenbach, C., Hideg, K., Krebs, M., Khorana, H. G., & Hubbell, W. L. (1994) *Science 266*, 105−107.
Tidor, B., & Karplus, M. (1991) *Biochemistry 30*, 3217−3228.
Timofeev, V. P., & Tsetlin, V. I. (1983) *Biophys. Struct. Mech. 10*, 93−108.
Timofeev, V. P., & Samarianov, B. A. (1993) *Appl. Magn. Reson. 4*, 523−539.
Tsugita, A., Inouye, M., Terzaghi, E., & Streisinger, G. (1968) *J. Biol. Chem. 248*, 391−397.
Van, S. P., Birrell, G. B., & Griffith, O. H. (1974) *J. Magn. Reson. 15*, 444−459.
Weaver, L. H., & Matthews, B. W. (1987) *J. Mol. Biol. 193*, 189−199.
Weaver, L. H., Gray, T. M., Grütter, M. G., Anderson, D. E., Wozniak, J. A., Dahlquist, F. W., & Matthews, B. W. (1989) *Biochemistry 28*, 3793−3797.
Wynn, R., & Richards, F. M. (1993) *Protein Sci. 2*, 395−403.
Zhang, X.-J., Baase, W. A., & Matthews, B. W. (1991) *Biochemistry 30*, 2012−2017.
Zhang, X.-J., Baase, W. A., & Matthews, B. W. (1992) *Protein Sci. 1*, 761−776.
Zhang, X.-J., Wozniak, J. A., & Matthews, B. W. (1995) *J. Mol. Biol. 250*, 527−552.

BI960482K